Chinese Journal of
POLYMER SCIENCE

RESEARCH ARTICLE

https://doi.org/10.1007/s10118-021-2635-7
Chinese J. Polym. Sci. **2022**, *40*, 93–106

Influence of Interfacial Enantiomeric Grafting on Melt Rheology and Crystallization of Polylactide/Cellulose Nanocrystals Composites

Hua-Gao Fang[a,b*], Kang-Jie Yang[a], Qi-Zheng Xie[a], Xu Chen[a], Sheng-Li Wu[a,c*], and Yun-Sheng Ding[a,b*]

[a] *Department of Polymer Science and Engineering, School of Chemistry and Chemical Engineering, Hefei University of Technology, Hefei 230009, China*
[b] *Anhui Province Key Laboratory of Advanced Functional Materials and Devices, Hefei 230009, China*
[c] *Anhui Institute for Food and Drug Control, Hefei 230051, China*

Electronic Supplementary Information

Abstract Incorporating the surface-grafted cellulose nanocrystals (CNCs) with enantiomeric polylactide (PLLA or PDLA) is an effective and sustainable way to modify PLLA, but their difference in promoting matrix crystallization is still unrevealed. In this study, the CNCs with identical content and length of PLLA and PDLA (CNC-*g*-L and CNC-*g*-D) were prepared and blended with PLLA. The rheological properties of PLLA/CNC-*g*-D are greatly improved, indicating that the stereocomplexation can significantly improve the interfacial strength as compared with the conventional van der Waals force in PLLA/CNC-*g*-L. Surprisingly, the matrix crystallizes at a higher rate in PLLA/CNC-*g*-L than PLLA/CNC-*g*-D. PLLA/CNC-*g*-L15 reaches its half crystallinity in 8.26 min while a longer period of 13.41 min is required for PLLA/CNC-*g*-D15. POM observation reveals that the superior crystallization behavior in PLLA/CNC-*g*-L is originated from its higher nucleation efficiency and faster growth rate. The formation of low content of sc-PLA at the interface can restrict the diffusion of PLLA but contribute less to generate crystalline nuclei, which synergistically leads to the retarded crystallization kinetics in PLLA/CNC-*g*-D. Revealing the mechanism of different interfacial enantiomeric grafting on the melt rheology and crystallization of PLLA is of great significance for the development of high-performance polylactide materials.

Keywords Cellulose nanocrystal; Polylactide nanocomposite; Interfacial stereocomplexation; Crystallization; Rheology

Citation: Fang, H. G.; Yang, K. J.; Xie, Q. Z.; Chen, X.; Wu, S. L.; Ding, Y. S. Influence of interfacial enantiomeric grafting on melt rheology and crystallization of polylactide/cellulose nanocrystals composites. *Chinese J. Polym. Sci.* **2022**, *40*, 93–106.

INTRODUCTION

Polylactide is a type of aliphatic thermoplastic polyester and made from green plant materials. Due to the characteristics of biodegradability, biocompatibility, processability, and economical efficiency, it has been used as the most promising alternative in food packaging film, tissue repairing, foaming materials and other fields.[1–5] However, polylactide itself is brittle, has a low glass transition temperature, and a slow crystallization rate, resulting in insufficient mechanical strength and poor heat resistance, which seriously limits the expansion of application.[6–8] In order to improve the crystallization kinetics of polylactide, the commonly used method is to add a nucleating agent or a plasticizer. Adding a nucleating agent can reduce the free energy barrier of the nucleation surface of polylactide and increase the crystallization rate of polylactide.[9–11] Plasticizers can reduce the glass transition temperature and increase the mobility of the chain segments, thereby accelerating its crystallization.[12,13]

Cellulose nanocrystals (CNCs) are non-toxic, biodegradable nanoparticles that can be obtained from many renewable resources such as wood, cotton, and algae. CNCs show the characteristics of high rigidity, low density, large aspect ratio and biodegradability, and have great potential to act as a green reinforcing filler for polymer materials.[14–18] When CNCs are used to modify PLA, because of the abundant hydrophilic hydroxyl groups on surface, the strong polarity causes poor compatibility and serious agglomeration in the matrix, which ultimately leads to the inferior comprehensive performance of the composites. Improving the dispersion of CNCs in the matrix and generating strong interfacial strength are the keys to successful modification in PLA/CNCs composites. Surface hydrophobic modification of CNCs can improve its dispersion and interface strength in the PLA matrix.[19–22] There are two ways to achieve the goal in the literature. One is to use non-covalent interactions such as electrostatic attraction, hydrogen bonding, and van der Waals forces, such as adsorption of surfactants,[23,24] polyelectrolyte adsorption,[25,26] *etc*. The other method is the chemical reaction on the CNCs surface, including esterification, oxidation, silanization, and polymer grafting.[27–31]

Surface grafting of homogeneous polymer segments to im-

* Corresponding authors, E-mail: fanghg@hfut.edu.cn (H.G.F.)
E-mail: wazxh526@163.com (S.L.W.)
E-mail: dingys@hfut.edu.cn (Y.S.D.)

Received July 1, 2021; Accepted August 4, 2021; Published online November 4, 2021

prove the compatibility with the matrix is a straightforward philosophy in polylactide nanocomposites. When CNCs were grafted with poly(L-lactide) (PLLA), they can improve the dispersion in the matrix and act as a nucleating agent to enhance the crystallization ability of the matrix.[32] Lizundia[33] and de Paula[34] *et al*. grafted PLLA on the surface of CNCs and used calorimetric method to study the crystallization behaviors of the grafted CNC-*g*-PLLA and PLLA composites, revealing that after adding CNC-*g*-PLLA, the crystallization temperature decreased and the final crystallinity was improved. The formation of stereocomplex crystallites (sc-PLA) between enantiomeric chains is a unique phenomenon in polylactide materials, PLLA and poly(D-lactide) (PDLA) chains interact with each other through intermolecular hydrogen bonds, which causes the denser chain packing in the crystal lattice of sc-PLA than that in the homocrystallites formed by enantiopure PLLA or PDLA. The sc-PLA formed by the CNCs grafted with PDLA and the PLLA matrix also proved to be a heterogeneous nucleating agent that promotes the crystallization of PLLA. Habibi *et al*.[35] prepared CNC-*g*-PDLA by the ring-opening polymerization of D-lactide on the surface of CNCs, and its PLLA-based nanocomposites by melt blending. They reported that with the increase of CNC-*g*-PDLA content, the crystallization capability of nanocomposites gradually increased, and the mechanical properties were also significantly improved compared to those of neat PLA. This was all ascribed to the formation of sc-PLA at the interface, which not only acted as nucleating agents to promote the matrix crystallization but also leaded a physical network in the composites to improve the mechanical strength. In addition, other studies have shown that incorporating PDLA-grafted nanofillers into the PLLA matrix would form sc-PLA and restrict the formation of homogeneous PLA crystals. For example, Arvind and coworkers[36] filled the microcrystalline cellulose (CWC) grafted with PDLA into the PLLA matrix to study the gas barrier and thermomechanical properties. With the increase of CWC content, the X-ray diffraction peaks of homogeneous crystals gradually disappeared, and the diffraction peaks of stereocomplex crystals gradually increased, indicating that the addition of CWC-*g*-PDLA brought hindering effects on the formation of homogeneous crystallites. Zhang and coworkers[37] reported the synthesis and characterization of CNC-*g*-PDLA and its nanocomposite with PLLA. Their results showed that the addition of small amount of CNC-*g*-PDLA could enhance the crystallization rate of PLLA significantly due to the heterogeneous nucleation effect of CNCs and the presence of stereocomplex crystals. In addition, the specific stereocomplex interaction in the interphase of PLLA matrix and modified CNC particles results in great improvement of both storage modulus and the heat distortion resistance of the PLLA/CNC-*g*-PDLA nanocomposites. Our previous work also showed that the surface grafting of PDLA can improve the thermal stability and dispersion of CNCs in PLLA matrix and PLLA containing polyurethane, leading to significant improvement of mechanical and barrier properties.[38–40]

From the above review, we can find that after surface-grafted with PLLA or PDLA, both type of CNCs can promote the dispersion and crystallization of the matrix, but their promoting efficiency is still unclear. In this work, we particularly prepared CNCs grafted with the identical content and length of PLLA and PDLA on the surface and compared the rheological and crystallization properties of their PLLA composites, aiming to clarify the effect of the different interfacial interactions, which are the conventional van der Waals force and the stereocomplex interaction in sc-PLA, on the structure and performance of PLA/CNCs composites and thus deepen the understanding of PLA and CNCs nanocomposites.

EXPERIMENTAL

Materials

Cotton linters was obtained from Hubei Chemical Fiber Group Co., Ltd., (Xiangfan, China). L-lactide (LLA) and D-lactide (DLA) were purchased from Jinan Daigang Biotechnology Co., Ltd., (Jinan, China). Polylactide (PLLA, 4032D) was purchased from NatureWorks (USA), in which the content of LLA is about 98.6%. Ethyl acetate, sulfuric acid, toluene, methanol, chloroform, and acetone were purchased from Sinopharm Chemical Reagent Co., Ltd., (Shanghai, China). Ethyl acetate and toluene were purified before use. Tin(II) 2-ethylhexanoate ($Sn(Oct)_2$, 95%) was purchased from Sigma-Aldrich (Shanghai, China).

Preparation of CNC-*g*-D and CNC-*g*-L

The CNC particles were isolated from cotton linters according to the similar procedure in our previous work.[39] The PDLA grafted CNCs sample (CNC-*g*-D) was prepared by surface initiated ring-opening polymerization of D-lactide and described as follows: 70 mL of acetone was mixed with 35 mL of CNCs suspension in water (20 mg·mL^{-1}), then mechanically stirred for 30 min, and the nanoparticles were further dispersed using an ultrasonic crusher with the amplitude of 40%. The mixture was centrifuged at 6000 r/min for 5 min, and then the supernatant was removed and washed for three times with acetone and dry toluene, respectively. Subsequently, 200 mL of anhydrous toluene was added, and sonicated for another 30 min to improve the dispersion. The obtained suspension was azeotropically boiled for 30 min to remove residual water. Purified D-lactide (30 g) was added and $Sn(Oct)_2$ was used as the catalyst. The polymerization was continued at 80 °C for 24 h and terminated by the addition of several drops of diluted hydrochloric acid solution. The resulting suspension was added dropwise into cold methanol, and the precipitate was collected. The resulting precipitate was washed for three times with chloroform and dried in a vacuum oven at 60 °C for 24 h. The final sample was named CNC-*g*-D. The same method was adopted to prepare CNC-*g*-L by changing the type of lactide.

Preparation of PLLA Nanocomposites

The PLLA nanocomposites using CNC-*g*-L and CNC-*g*-D as the fillers were prepared by the solution casting method. First, the weighted CNC-*g*-D was dispersed into chloroform with the aid of sonication in a cell crusher. Second, the dispersion was mixed with the chloroform solution of PLLA, stirred mechanically and placed in a fume hood to evaporate the solvent. The obtained films were transferred into a vacuum oven at 60 °C for 48 h to remove the residual solvent. The mass fractions of CNC-*g*-D in the composite were 5% and 15%, and named as PLLA/CNC-*g*-D5 and PLLA/CNC-*g*-D15, respectively. The PLLA/CNC-*g*-L composites were prepared using the same procedure and named as PLLA/CNC-*g*-L5 and PLLA/CNC-*g*-L15,

https://doi.org/10.1007/s10118-021-2635-7

respectively.

Characterization

Fourier transform infrared spectroscopy (FTIR)

FTIR measurements on the CNCs samples were carried out on a Nicolet Nexus 67 FTIR (Thermo Scientific, USA) at room temperature. The scanning range is 4000–400 cm^{-1}. Before the measurement, the samples were dried in a vacuum oven at 60 °C for 24 h.

Proton nuclear magnetic resonance (^{1}H-NMR)

After ultrasonication, the dispersion of grafted CNCs in deuterated chloroform was measured immediately on a Varian (Agilent, USA) 600 MHz NMR spectrometer.

Wide-angle X-ray diffraction (WAXD)

WAXD measurements were carried out using X'Pert PRO MPD X-ray diffraction. The measurements were operated at 40 kV and 40 mA with scan angles from 4° to 28° at a scan rate of 2 (°)·min^{-1}.

Differential scanning calorimetry (DSC)

The DSC measurement was performed on a TA-Q2000 DSC instrument (TA Instruments, USA). During the non-isothermal crystallization process, about 5 mg of sample was heated to 180 °C at a heating rate of 10 °C·min^{-1} under a nitrogen atmosphere, and kept at this temperature for 5 min to eliminate possible crystallites, and then cooled down to 0 °C at a cooling rate of 10 °C·min^{-1}, and finally heated again from 0 °C to 240 °C at a heating rate of 10 °C·min^{-1}. By measuring the cold crystallization temperature (T_c), the melting point of homogeneous crystals ($T_{m,HC}$), the melting point of sc-PLA crystallites ($T_{m,SC}$), the cold crystallization enthalpy (ΔH_{cc}), and the melting enthalpy of homogeneous crystals ($\Delta H_{m,HC}$) and the melting enthalpy ($\Delta H_{m,SC}$) of SC-PLA crystallites, the relative crystallinity (χ_c) of PLLA matrix in the nanocomposites was analyzed using the following equation (Eq. 1):

$$\chi_c = \frac{\Delta H_m - \Delta H_{cc}}{w_f \Delta H_m^0} \times 100\% \quad (1)$$

where w_f is the mass fraction of PLLA and ΔH_m^0 is the melting enthalpy of PLLA under 100% crystallization conditions. In this study, 93.6 J·g^{-1} was selected as the melting enthalpy.[41]

During the isothermal crystallization process, the sample was kept at 180 °C for 5 min to remove possible homo-crystallites and preserve interfacial sc-PLA. After that, the sample was cooled to 130, 135, and 140 °C at a cooling rate of 30 °C·min^{-1} and maintained at this temperature until the crystallization was completed. The thermal flow curve during the process was recorded to calculate the crystallization kinetics. The relative crystallinity (χ_t) at a specific crystallization time (t) is obtained by integrating and normalizing the exothermic curve during the crystallization process. The specific calculation equation is as follows:

$$\chi_t = \frac{\int_0^t dH_c/dt dt}{\int_0^{t=\infty} dH_c/dt dt} \times 100\% \quad (2)$$

Polarized light microscopy

Using a polarized light microscope (POM, Olympus-BX53) equipped with a CCD camera, the nucleation and spherulite growth of the samples were observed. The sample film was prepared by solution casting method and dried in a vacuum oven at 60 °C for 24 h before observation. The film was melted at 180 °C for 5 min to eliminate the thermal history, and then quickly transferred to the hot stage at the pre-setted temperature to observe the isothermal crystallization process.

Rheology measurement

Rheological measurements were performed on a stress-controlled Malvern Kinexus rotational rheometer using an 8 mm plate-plate geometry at 180 °C with frequencies ranging from 0.1 rad/s to 100 rad/s at a strain amplitude of 1%. The geometry gap was maintained at 0.5 mm and nitrogen protection was applied to minimize possible degradation.

RESULTS AND DISCUSSION

Preparation and Characterization of CNCs with Different Chiral Polylactides

In the surface grafting process, the hydroxyl groups on the CNCs surface were used to initiate the ring-opening polymerization of lactide and the mass ratio of CNCs to lactide was particularly controlled to be the same in preparation of CNC-*g*-D and CNC-*g*-L (Fig. 1a). The successful grafting with PLA segments on CNCs surface was verified using FTIR measurements in Fig. 1(b). As compared with the pristine CNCs, both CNC-*g*-D and CNC-*g*-L show a new band at 1750 cm^{-1}, which corresponds to the carbonyl stretching vibration of PLA. The grafting content of CNC-*g*-L and CNC-*g*-D were analyzed by the method reported previously.[37] Figs. 1(c) and 1(d) show the FTIR spectra of the grafted sample in the range of 1500–1400 cm^{-1}, in which the band at 1454 cm^{-1} corresponding to the stretching vibration of the methyl group on PLA and the band at 1430 cm^{-1} to the bending vibration of the methylene group on CNCs. The ratio of peak intensity I_{1430} to I_{1454} can reflect the grafting content of PLA on the CNCs surface. The obtained grafting contents are 41.5% and 39.3% on CNC-*g*-L and CNC-*g*-D, respectively, calculated from the relation $Y = 0.139X + 0.035$ (Y represents the ratio to I_{1430} and I_{1454}, and X represents the mass ratio to CNCs and PLA).[42] The high grafting of PLA contributes to the improved dispersion of former hydrophilic CNCs in a hydrophobic medium. As shown in Fig. 1(e), the pristine CNCs completely settle down in chloroform after 24 h, while the two surface-modified CNCs sample dispersion can remain stable for the same period of time.

Besides, the grafting length is also an important factor affecting the interfacial layer between CNCs and the PLLA matrix. We carefully analyzed the molecular weight of surface grafting by DSC and ^{1}H-NMR method. The empirical relation of the melting point and molecular weight was utilized to estimate the chain length of PLA (Eq. 3):[43,44]

$$T_m = T_m^\infty - \frac{A}{M_n} \quad (3)$$

where T_m is the melting point of grafted PLA, shown in Fig. 1(f), T_m^∞=181.3 °C, and constant A=1.02×10^5 °C g·mol^{-1}. The obtained grafting molecular weights of CNC-*g*-D and CNC-*g*-L are 858.6 and 827.9 g·mol^{-1}, respectively. It should be noted that the crystallization of polymer could be restricted on the surface of CNCs, leading to decreased lamellar thickness and less crystalline perfection. These molecular weights could be underestimated because the obtained melting point of crystallinites is lower than that from bulk state.

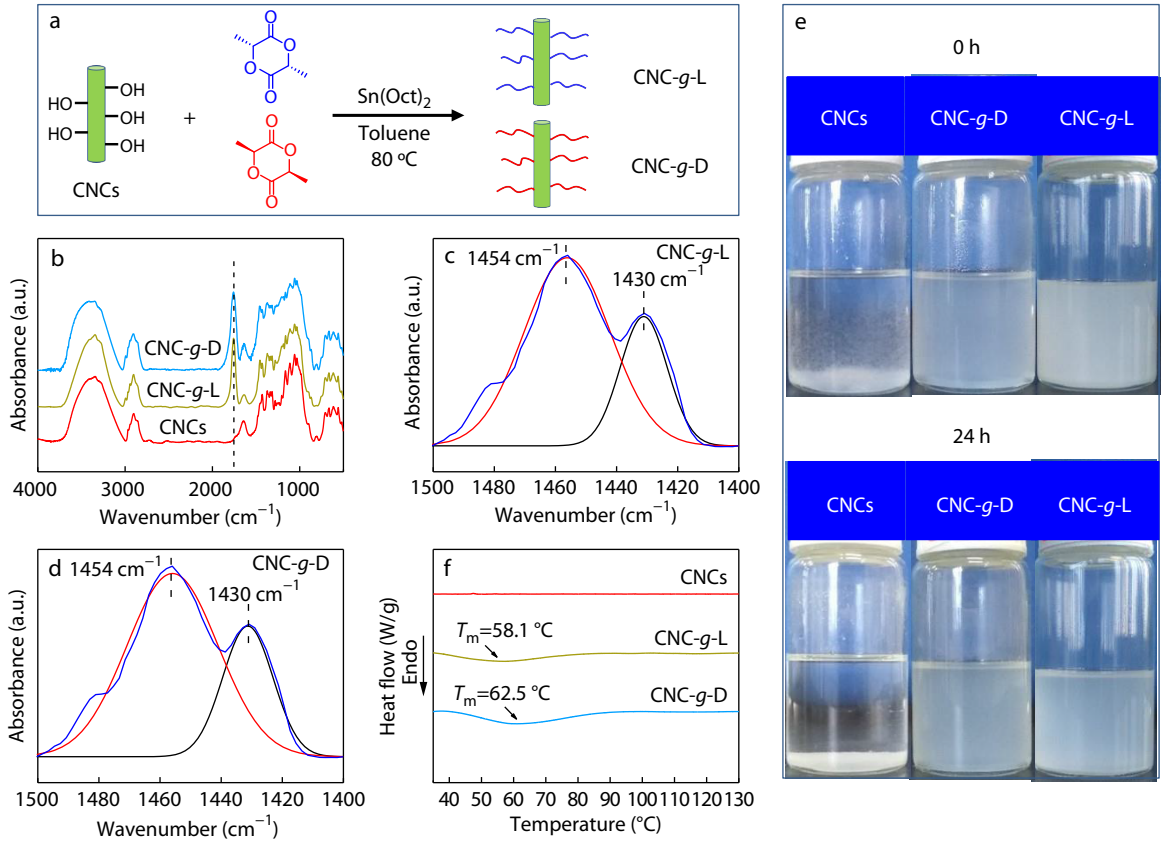

Fig. 1 Preparation and characterization of CNC-*g*-L and CNC-*g*-D.

For further verified the identical grafting length, ^{1}H-NMR of CNCs, CNC-*g*-D and CNC-*g*-L within the chemical shift range of 5.5–4.0 ppm were obtained and shown in Fig. S1 (in the electronic supplementary information, ESI). CNCs show an obvious characteristic peak at 5.35 ppm. After surface grafting, the peak area is markedly decreased and new peaks appear at 5.16 and 4.35 ppm, which correspond to the methine peak connecting the ester group and the methine peak near the terminal hydroxyl group on PLA, respectively. Accordingly, the relative intensities of the two peak areas can be used to obtain the molecular weights of PLA on CNC-*g*-D and CNC-*g*-L, which are 1458 and 1394 g·mol^{-1}, respectively. Although the values of molecular weight from above two methods are different due to varied measurement mechanism, the results strongly indicate that the CNCs particles with the same grafting PLLA and PDLA chain length were successfully obtained.

Melt Rheology

The polylactide composites incorporated with various amounts of CNC-*g*-L and CNC-*g*-D were prepared by the solution casting method. Their melt rheological properties were first investigated. Since the content and length of PLLA and PDLA on the surface of CNCs are identical and the molecular weight is far less than the critical entanglement molecular weight of PLA (about 8000 g·mol^{-1}), the entanglement between matrix and grafting chain is unlikely formed and the only interfacial difference is the conventional van der Waals force in PLLA/CNC-*g*-L and the stereocomplex interaction between enantiomeric PLA chains in PLLA/CNC-*g*-D. As shown in Figs. 2(a) and 2(b), the storage and loss modulus are improved after filling with surface-modified CNCs particles. The slope in the low-frequency end region also gradually decreases, strongly indicating the decreased relaxation of macromolecules. Compared with PLLA/CNC-*g*-L samples, the storage and loss modulus of PLLA/CNC-*g*-D series samples are both higher. It is worth noting that the modulus of the PLLA/CNC-*g*-D5 sample is even greater than that of PLLA/CNC-*g*-L15 sample, which indicates that CNC-*g*-D and the matrix PLLA have a higher modulus than CNC-*g*-L. After adding modified fillers to polylactide matrix, the viscosity of the samples shows increase to various degrees (Fig. 2c). The complex viscosity of PLLA/CNC-*g*-D sample is higher than that of PLLA/CNC-*g*-L sample, and with the further increase of the filling content, the viscosity of neat PLLA in the low frequency region basically remain unchanged within the shear frequency, and the shear thinning behavior does not appear until the higher frequency, which reflects the transformation process of Newtonian fluid to power law fluid. However, with the exception of PLLA/CNC-*g*-L5 and PLLA/CNCs samples, other PLLA composite materials exhibit a shear thinning process in the low frequency region. The shear thinning behavior is caused by the disentanglement and orientation of the matrix PLLA in the shear direction. The shift of transition point from power law to Newtonian flow to higher frequencies in the PLLA/CNC-*g*-D composite reflects the different interfacial interactions.[45,46] The phase angle tangent (tanδ) can characterize the solid-liquid transition behavior. It can be observed from Fig. 2(d) that tanδ of neat PLLA gradually increases as the frequency decreases, which is the terminal behavior for a typical linear polymer.

https://doi.org/10.1007/s10118-021-2635-7

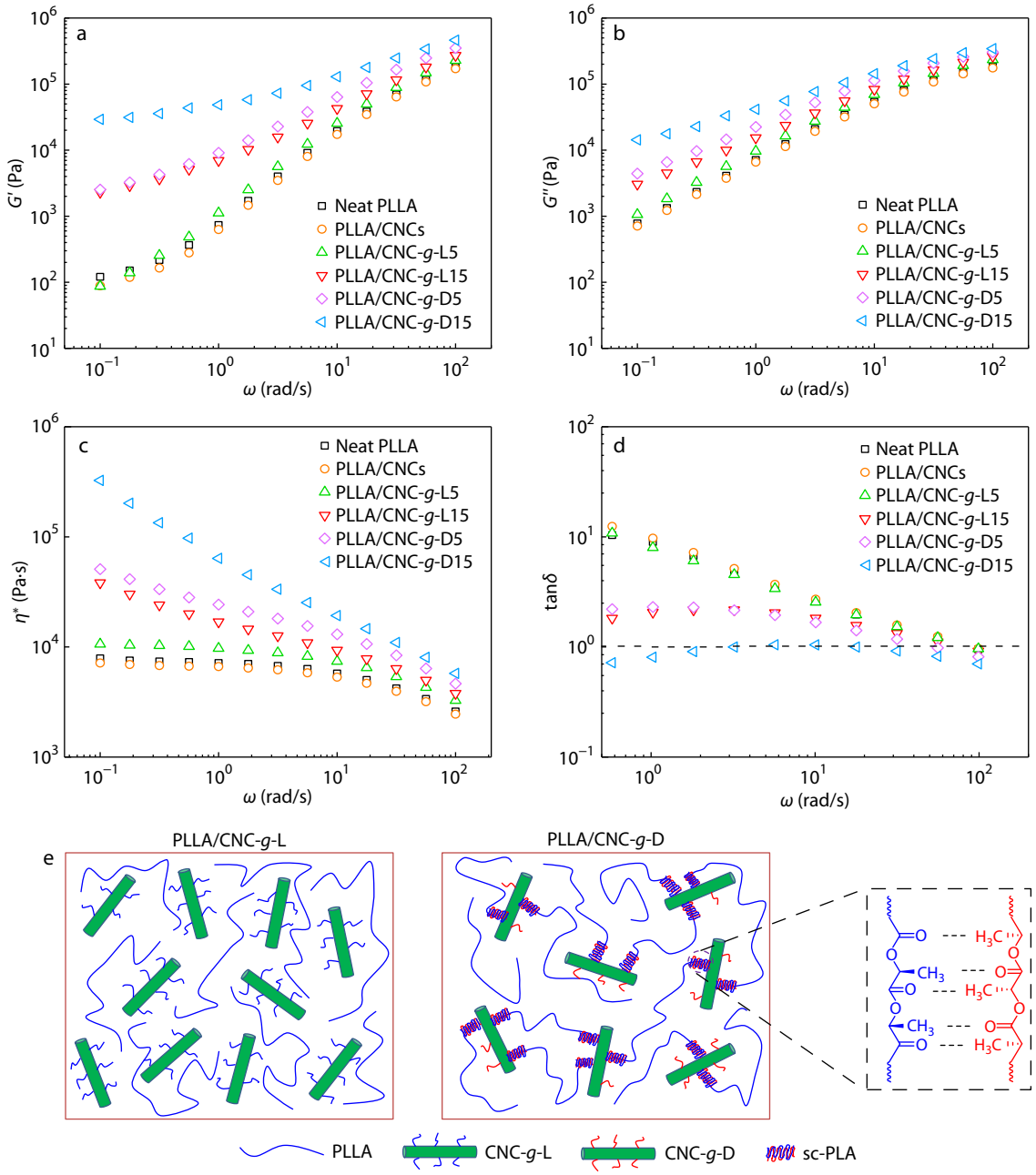

Fig. 2 (a) Storage (G'), (b) loss modulus (G''), (c) complex viscosity (η^*) and (d) phase angle tangent of neat PLLA and nanocomposites at 180 °C as a function of frequency, (e) schematic illustration of interfacial interaction in PLLA nanocomposites.

When the filler is introduced, tanδ in the low frequency range is reduced. Compared with PLLA/CNC-*g*-L samples, the tanδ of PLLA/CNC-*g*-D samples in the low frequency region is smaller, and further decreases as the filling content increases. It is worth noting that the tanδ of PLLA/CNC-*g*-D15 in the low frequency region is less than 1 and is independent on frequency. This indicates that the relaxation behavior of the matrix segment in PLLA/CNC-*g*-D15 undergoes a solid transformation, which may be due to the strong restriction of the sc-PLA and the percolation network formed between nanoparticles. The schematic illustration of the interfacial structure in the nanocomposite is shown in Fig. 2(e). In the PLLA/CNC-*g*-L samples, due to the short grafting molecular length, which is less than the critical entanglement molecular weight (M_e) of PLA, there is only conventional intermolecular van der Waals interactions between the PLLA matrix and CNCs. While in the PLLA/CNC-*g*-D samples, the strong interfacial interactions, originated from the stereocomplexation on the interface of CNCs and the PLLA matrix, restricted the movement and diffusion of the PLLA chains and contributed to the formation of a percolation network of CNCs, resulting in the great enhancement in rheological properties.[45]

Crystalline Structure Analysis

The crystalline structure of the polylactide composites is

characterized by WAXD and FTIR, as shown in Fig. 3. The WAXD results reveal that the diffraction peaks at 16.6° and 19.0° of PLLA samples correspond to the (110) and (203) crystal planes of the homogeneous crystal (HC), respectively. After adding the modified CNCs, new characteristic diffraction peaks appear in all composite materials at 14.8° and 22.7°, corresponding to the (110) and (200) crystal planes in CNCs, respectively.[16,47] The diffraction peak intensity of the composite material with high content of CNCs in the polylactide HC (110) crystal plane is higher than that with low content of CNCs. This shows that with the increase of CNCs content, its crystallization promotion effect on polylactide HC gradually increases. The WXRD spectrum of PLLA/CNC-*g*-D15 shows two new characteristic diffraction peaks at 12° and 21°, corresponding to the (110) and (300/030) crystal planes of sc-PLA, respectively. The different crystalline structures are also reflected in FTIR measurements. The two characteristic bands at 905 and 920 cm^{-1} of the composites correspond to the sc-PLA and HC at the interface, respectively.[48] All the composite materials show an obvious characteristic band at 920 cm^{-1}, but only PLLA/CNC-*g*-D15 shows a characteristic band of sc-PLA at 905 cm^{-1}. It is noted that due to the low content of sc-PLA, the characteristic band cannot be observed in PLLA/CNC-*g*-D5.

Thermal Property

The content of filler particles and the interface interaction are the key factors affecting the aggregate structure in the nanocomposite materials. In order to explore the effect of sc-PLA on the structure evolution of composite materials during thermal processing, we first explored the heating and cooling thermal behaviors in neat PLLA and the nanocomposites. In the non-isothermal test, we first intentionally heated the film samples at 180 ℃ to eliminate the possible HC while preserve the sc-PLA. The heat flows in cooling and second heating processes were recorded and are shown in Fig. 4. No remarkable change was observed after adding grafted CNCs, indicating the local segment motion was barely influenced by the

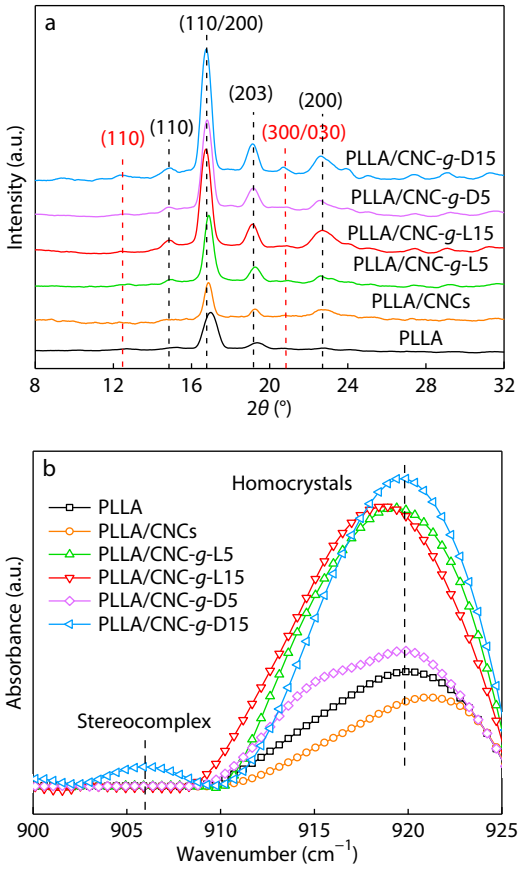

Fig. 3 (a) WAXD patterns and (b) FTIR spectra of neat PLLA and the nanocomposites.

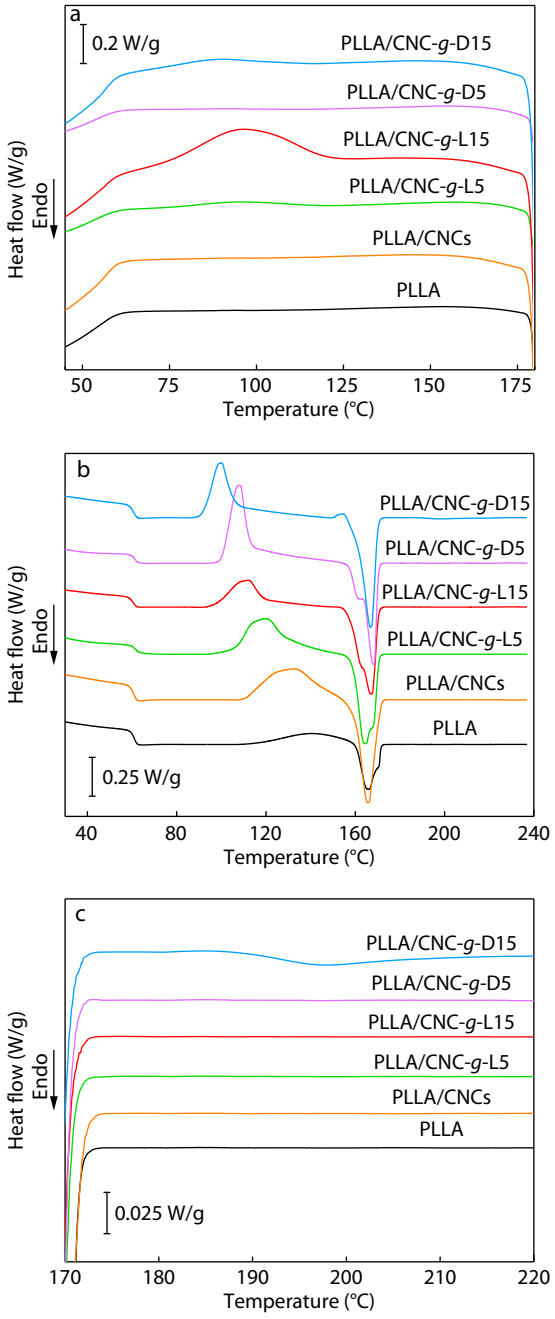

Fig. 4 DSC curves of neat PLLA and the nanocomposites during (a) the cooling scan, (b) the second heating scan, and (c) the magnified DSC curves in the second heating scan.

https://doi.org/10.1007/s10118-021-2635-7

nanoparticles. It can be seen from Fig. 4(a) that there is no melting crystallization phenomenon in neat PLLA during the cooling process. After adding the nanofillers, the melting crystallization of PLLA has been improved to some extent. For example, PLLA/CNC-*g*-L5 shows a melt crystallization peak at around 92.3 °C with incorporation of CNC-*g*-L. With the increase of filler content, the melt crystallization temperature of PLLA/CNC-*g*-L15 increases to 97.8 °C, and the peak area increases significantly. When CNC-*g*-D was added, PLLA/CNC-*g*-D5 does not show obvious crystallization exothermal peak during the cooling process. With the content increases, PLLA/CNC-*g*-D15 shows a melt crystallization peak at 92.5 °C, but the peak intensity is much lower than that of PLLA/CNC-*g*-L15. Since the contents of CNC-*g*-D and CNC-*g*-L are identical, the difference in melt crystallization may be caused by the difference in the interaction between the filler particles and the matrix. The strong interaction between CNC-*g*-D and PLLA matrix restricts the diffusion of PLLA, thereby limiting the melt crystallization. Fig. 4(b) shows the heat flow during the second heating process, in which the cold crystallization temperature (T_c), cold crystallization enthalpy (ΔH_{cc}), melting temperature (T_m), melting enthalpy (ΔH_m) and relative crystallinity (χ_c) are summarized in Table S1 (in ESI). It can be seen that the T_c of neat PLLA is the highest, and the double peak phenomenon appears when melting. The crystallinity of HC of neat PLLA after the second heating is determined to be only 1.6%. When the nanofillers are added, the cold crystallization occurs at lower temperature and higher relative crystallinity can be achieved. Compared with PLLA/CNC-*g*-L in the second heating process, PLLA/CNC-*g*-D possesses lower crystallization temperature and higher enthalpy value. This may be due to the fact that lower crystallinity in the PLLA/CNC-*g*-D samples after cooling. The relative crystallinity of PLLA/CNC-*g*-D series after second heating is much lower than that of PLLA/CNC-*g*-L series. It can be seen from Fig. 4(c) that the melting peak of sc-PLA only appears at around 197 °C in PLLA/CNC-*g*-D15, but does not appear in PLLA/CNC-*g*-D5 due to its low content.

It should be noted that although the PDLA grafted CNCs particles demonstrate higher efficiency in accelerating crystallization of PLLA than the pristine CNCs, it is less effective than the PLLA grafted particles, which seems to be different from the results in other PLA grafted nanoparticle systems. As reported by Fu and coworkers,[49] when the grafted multi-walled carbon nanotubes (MWCNTs) are added in PLLA matrix, the particles with PDLA grafting show higher efficiency in promotion of crystallization than PLLA grafting. For better illustrate the different mechanisms of surface grafting on crystallization, their isothermal melt crystallization behaviors were investigated and discussed in the following sections.

Isothermal Crystallization Kinetics by DSC

Isothermal crystallization kinetics were first investigated at 130, 135, and 140 °C using the calorimetric method. The exothermic curve and relative crystallinity as the functions of time are shown in Fig. 5. It can be seen that after adding nanofillers, the melt crystallization of all the composites is accelerated as compared with that of neat PLLA, showing higher rate with the increasing filler content. The composite samples with pristine CNCs have a lower crystallization rate at 130 °C than those with CNC-*g*-L and CNC-*g*-D. The PLLA/CNC-*g*-L samples with the same filler content have a higher crystallization rate than the PLLA/CNC-*g*-D samples, and the crystallization rate of PLLA/CNC-*g*-L5 is even faster than that of PLLA/CNC-*g*-D15. As the crystallization temperature increases, the crystallization rate of all samples slows down and the retarded crystallization kinetic in PLLA/CNC-*g*-D is much more remarkable at 140 °C. PLLA/CNC-*g*-D5 demonstrates slightly lower rate than that of PLLA/CNCs, and the crystallization of PLLA/CNC-*g*-D15 experiences a prolonged process, showing a slightly higher rate at the initial stage but the whole crystallization process is even longer than that of PLLA/CNC-*g*-L5.

The Avrami equation was used to analyze the isothermal crystallization kinetics and its expression is shown as follows (Eq. 4):

$$1 - \chi_t = \exp\left(1 - kt^n\right) \tag{4}$$

where χ_t is the relative crystallinity at the crystallization time t, n is the Avrami index, which is related to the nucleation mechanism and growth mode, k is the crystallization rate constant of the entire crystallization process. Taking the logarithm of both sides of the Avrami equation, plotting $\ln[-\ln(1-\chi_t)]$ versus $\ln t$, a straight line with a slope of n and an intercept of $\ln k$ can be obtained (Fig. 6). The obtained Avrami index and crystallization rate constant are shown in Table S2 (in ESI).

It can be seen that the n values of all samples at different isothermal crystallization temperatures are between 1.6 and 3, indicating the formation of imperfect nuclei.[50] The half crystallization time $t_{1/2}$ values of the composite materials are all shorter than that of neat PLLA (Fig. 7), confirming that the addition of CNCs fillers can accelerate the crystallization of PLLA matrix. When isothermally crystallized at 130 and 135 °C, the k value of PLLA/CNC-*g*-L15 is nearly 2 orders of magnitude higher than that of neat PLLA, and the half crystallization time $t_{1/2}$ is also greatly shortened, *e.g.* the time is only 4.56 min at 130 °C. And at 135 °C, PLLA/CNC-*g*-L15 reaches its half crystallinity in 8.26 min while a longer time of 13.41 min is required for PLLA/CNC-*g*-D15, indicating less effective for the PDLA grafted CNCs in promoting matrix crystallization. The internal mechanism will be discussed in the following sections.

Isothermal Crystallite Evolution Revealed by POM

The nucleation and growth of crystallites are crucial in determining crystallization kinetics. In this study, the crystalline morphology and growth process of PLLA/CNCs nanocomposites at various temperatures were investigated by POM and the isothermal crystallite evolution at 130 °C are shown in Fig. 8. The incorporation of CNC-*g*-L and CNC-*g*-D has no effect on the morphology of crystallites, all demonstrating the spherulitic morphology at various filler contents. As compared with neat PLLA, the number of spherulites in all the nanocomposites has increased significantly. The spherulites of PLLA/CNC-*g*-L15 and PLLA/CNC-*g*-D15 can occupy the entire observation field within 10 min, while PLLA/CNC-*g*-L5 and PLLA/CNC-*g*-D5 cannot grow over the entire observation field until 16 and 20 min, respectively, indicating that the high content of filler has a stronger promoting effect on nucleation. Compared with PLLA/CNC-*g*-D15, the higher density of spherulites can be observed in PLLA/CNC-*g*-L15 in 2 min, which is due to the

https://doi.org/10.1007/s10118-021-2635-7

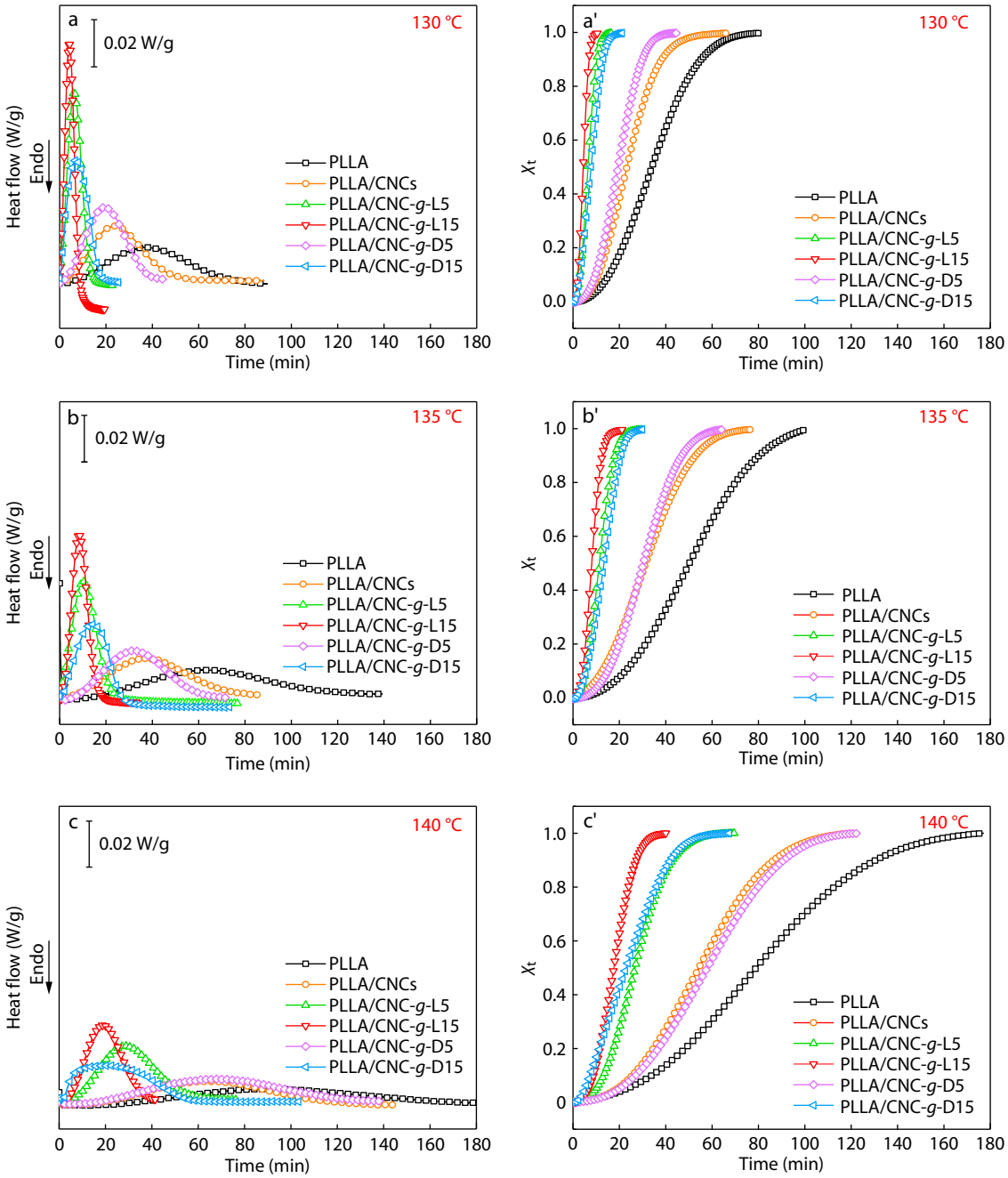

Fig. 5 (a–c) DSC curves and (a'–c') the relative crystallinity (χ_t) as functions of time during the isothermal crystallization of neat PLLA and the nanocomposites.

heterogeneous nucleation of CNC-*g*-L fillers, which reduces the energy barrier of formation of nuclei and accelerates the crystallization process. Although CNC-*g*-D also shows heterogeneous nucleation effect, its efficiency seems to be lower than CNC-*g*-L.

The changes of spherulite radius as functions of time at T_cs of 130, 135 and 140 °C for neat PLLA and the nanocomposites with 5 wt% fillers can be determined, as shown in Fig. 9. It can be observed that the PLLA spherulites grow with time linearly and from the slopes of the linearly fitted lines the spherulitic growth rates can be obtained. The spherulitic growth rates for neat PLLA, PLLA/CNC-*g*-L5 and PLLA/CNC-*g*-D5 at 130 °C are evaluated to be 1.77, 2.52 and 2.31 μm/min, respectively. The growth rates decrease with increasing temperature but the relative magnitude remains unchanged for three samples. On one hand, the incorporation of grafted CNCs particles can obviously accelerate the growth rate of PLA spherulites, which is consistent with the reports by other individual group.[51] On the other hand, due to the restrict effect of interfacial sc-PLA indicated by the higher viscosity in PLLA/CNC-*g*-D series, the movement and diffusion of PLLA chains were moderately retarded, leading to the reduced

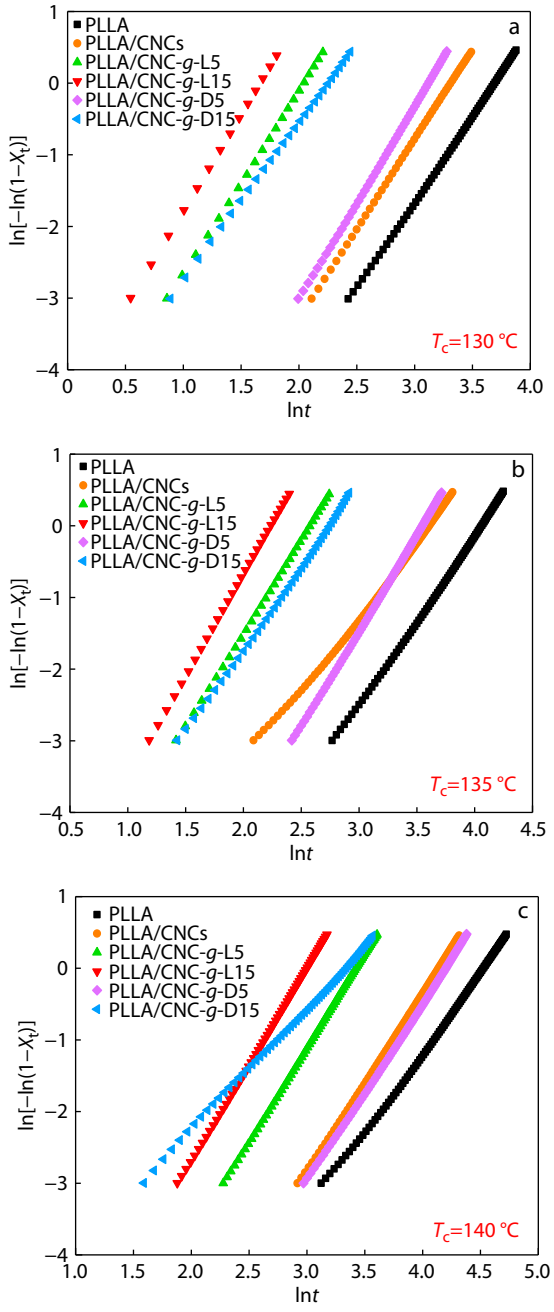

Fig. 6 Avrami plots for isothermal crystallization at different temperatures for neat PLLA and the nanocomposites: (a) 130 °C, (b) 135 °C and (c) 140 °C.

growth rate of PLA spherulites.

Nucleation Efficiency of the Grafted CNCs

The isothermal POM images at various crystallization temperatures are further shown in Fig. 10 to demonstrate the nucleation of grafted CNCs particles. Reduced nucleation density at higher temperature is observed for each PLLA composite, which is consistent with other polymer composites.[52–54] A close comparison reveals that PLLA/CNC-*g*-L series have a stronger ability to promote the nucleation of the PLLA matrix at all temperatures.

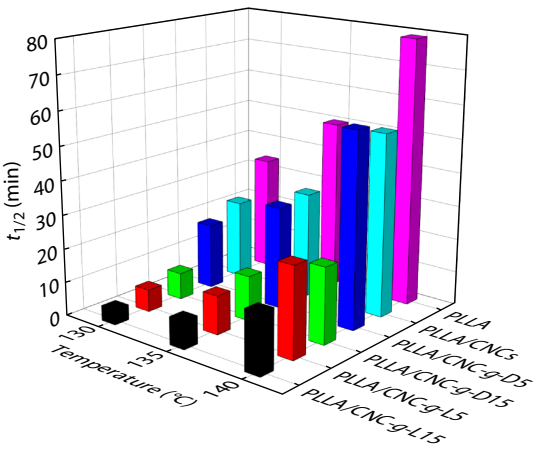

Fig. 7 Changes of half crystallization time ($t_{1/2}$) as functions of the crystallization temperature for neat PLLA and the nanocomposites.

The promoting efficiency of grafted CNCs particles on nucleation is quantitatively evaluated. The modified Avrami equation (Eq. 5) can be used to describe the volume filling effect of the spherulite growth process.[55,56] If the crystalline polymer is regarded as growing particles suspended in an amorphous matrix, the increase in crystallinity can be attributed to the volume filling effect of the crystal. There is a premise that all crystal nuclei N are generated at the same time t_0, and the growth rate of spherulites $G(t)$ is constant throughout the process, which has been verified by our POM observation. In our experiments, most of the nucleation occurred after quenching, and the spherulites start to grow at the set isothermal crystallization temperature. The crystal morphology observed by the polarizing microscope indicates that the crystal type remains the same during the isothermal process, and with the extension of the isothermal time, the second acceleration of crystallization kinetics does not appear. Therefore, it is appropriate to use this method to determine the density of spherulites generated by incorporation of grafted CNCs particles.

$$\phi(t) = 1 - \exp\left[-\frac{3}{4}\pi N G(t)^3 (t - t_0)^3\right] \quad (5)$$

Assuming that all crystal nuclei appear instantaneously when quenched to a certain isothermal temperature, the nucleation density of PLLA composites at different isothermal temperatures can be estimated using the volume filling degree in the modified equation (Eq. 6):

$$N = \frac{-3\ln[1 - \phi(t)]}{4\pi G(t)^3 t^3} \quad (6)$$

The changes of nucleation density as functions of space filling are shown in Fig. S2 (in ESI). It can be seen that the density of spherulites basically remains unchanged when the volume filling degree is between 0.1 and 0.9. Therefore, for the sake of convenience, we take the spherulite density when the volume filling degree is 0.5 as the nucleation density of neat PLLA and the nanocomposite. The nucleation density of the sample when the volume filling degree is 0.5 is summarized in Fig. 11. The reliability of this method is verified by the consistent nucleation density from Avrami modeling with the direct observation from POM. Note that the method of ob-

https://doi.org/10.1007/s10118-021-2635-7

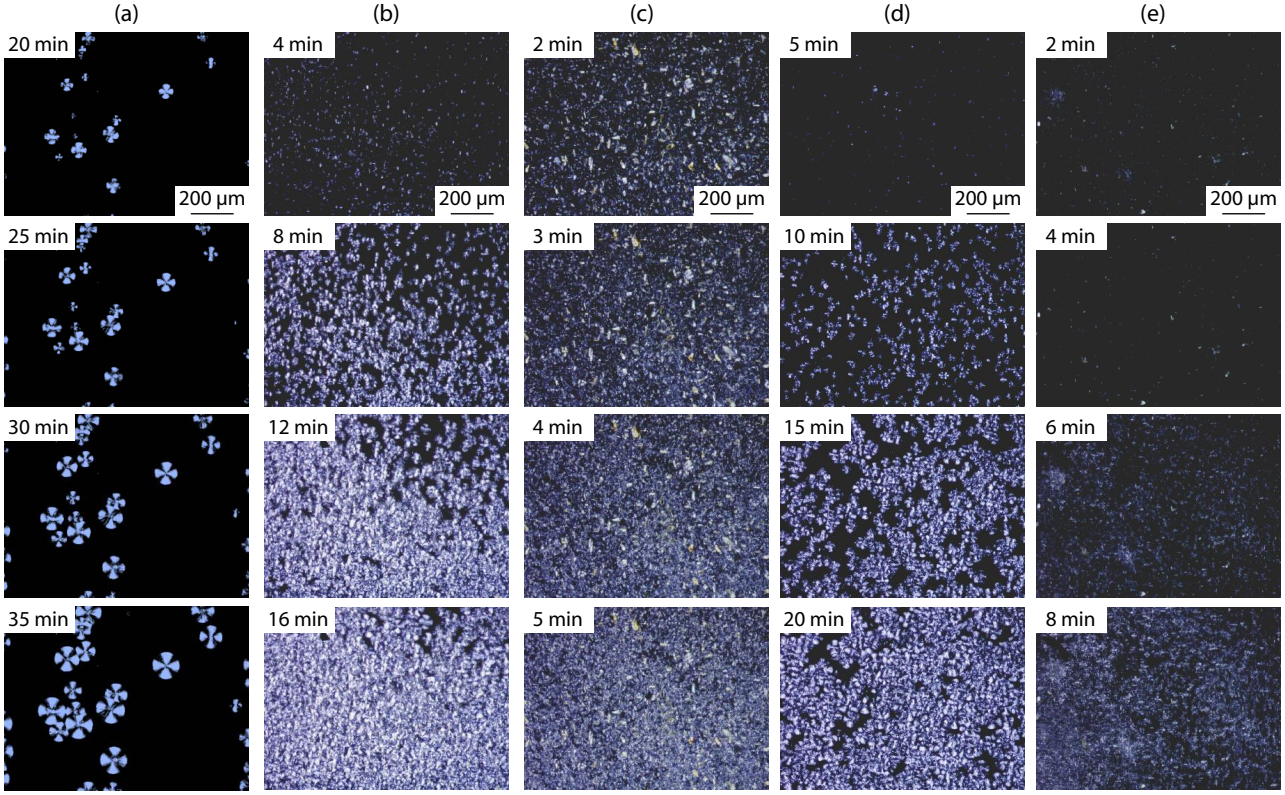

Fig. 8 POM images of isothermal crystallization of polylactide composite at 130 °C: (a) PLLA, (b) PLLA/CNC-*g*-L5, (c) PLLA/CNC-*g*-L15, (d) PLLA/CNC-*g*-D5, (e) PLLA/CNC-*g*-D15.

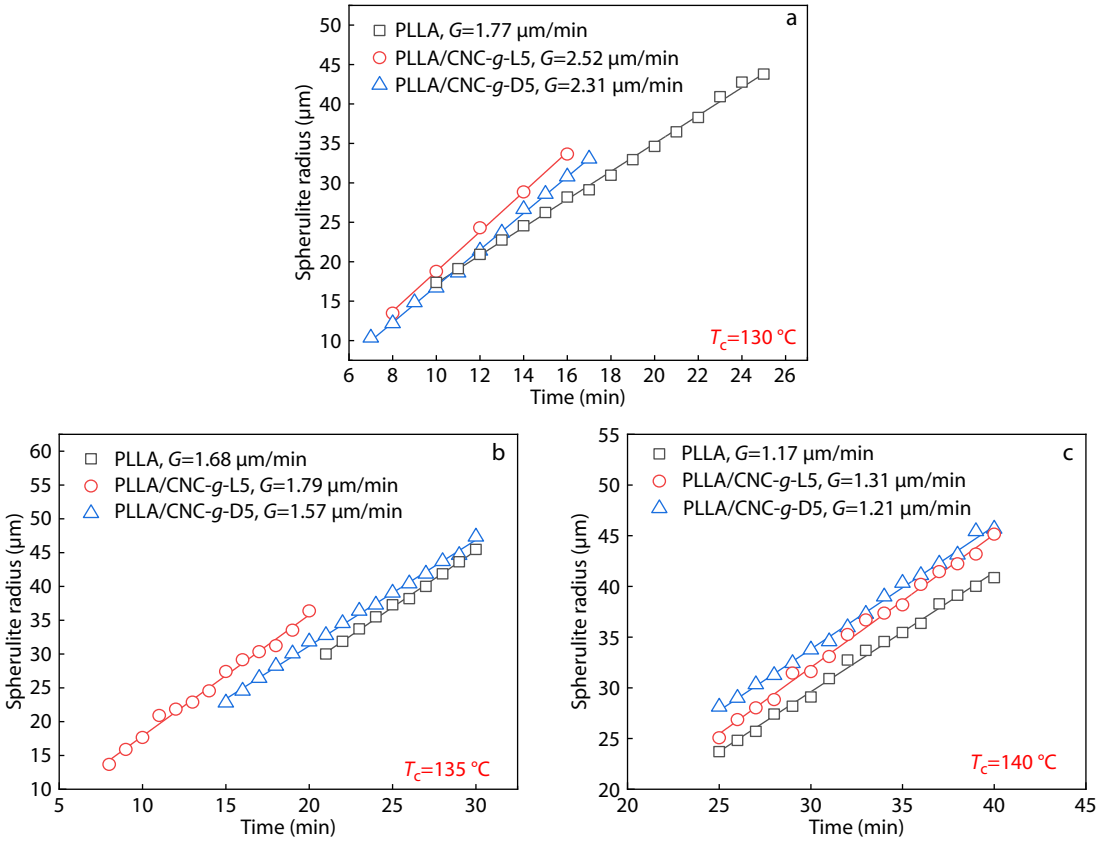

Fig. 9 Changes of spherulite radius as functions of time for neat PLLA and the nanocomposites at (a) 130 °C, (b) 135 °C and (c) 140 °C.

https://doi.org/10.1007/s10118-021-2635-7

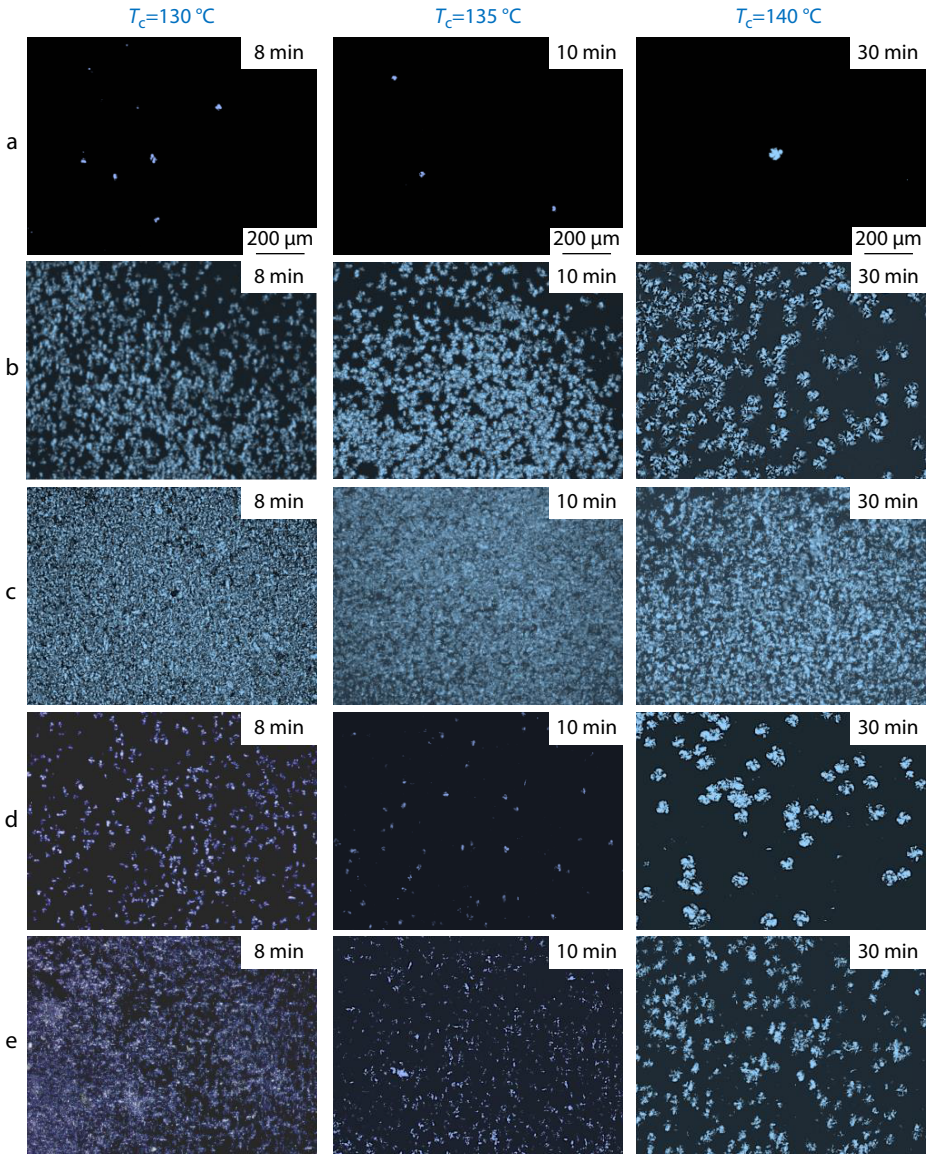

Fig. 10 POM images for (a) PLLA, (b) PLLA/CNC-*g*-L5, (c) PLLA/CNC-*g*-L15, (d) PLLA/CNC-*g*-D5, and (e) PLLA/CNC-*g*-D15 at various temperatures.

taining the nucleation density from POM is as follows: the number of spherulites in a certain area on the image was counted, the volume density can be calculated from the surface density using the empirical formula (Eq. 7):

$$N_V\left(m^{-3}\right) = N_A\left(m^{-2}\right)^{3/2} \quad (7)$$

It is obvious in Fig. 11 that PLLA/CNC-*g*-L5 shows a decade higher in nucleation than PLLA/CNC-*g*-D5, indicating the stronger promoting effect of CNC-*g*-L particles. In the nanocomposite, the modified CNCs act as the heterogeneous nucleating agents, which will reduce the nucleation induction period and increase the number of primary nucleation sites. Heterogeneous nucleation occurs when polymers are adsorbed on the surface of solid impurities to form crystal nuclei. Unlike the PDLA grafted MWCNTs, our PDLA grafted CNCs particles demonstrated less effective in nucleation than the PLLA grafted CNCs particles. Although the exact reason is not yet clear at this moment, it is possibly ascribed to the fact that the grafting length on our CNCs particles is short and the low content of sc-PLA formed between CNC-*g*-D and PLLA matrix cannot achieve its contribution in nucleation promotion.

CONCLUSIONS

Combined the isothermal DSC and POM investigation, the isothermal crystallization of PLLA/CNC-*g*-L series and PLLA/CNC-*g*-D series shows remarkable discrimination, which is originated from the difference in interfacial interaction for the identical grafting details. The conventional van der Waals force exists in PLLA/CNC-*g*-L and the stereocomplex interaction between enantiomeric PLA chains is formed in PLLA/CNC-*g*-D. The stereocomplex interaction leads to the orderly packing of enantiomeric PLA chains, which is verified by characteristic

https://doi.org/10.1007/s10118-021-2635-7

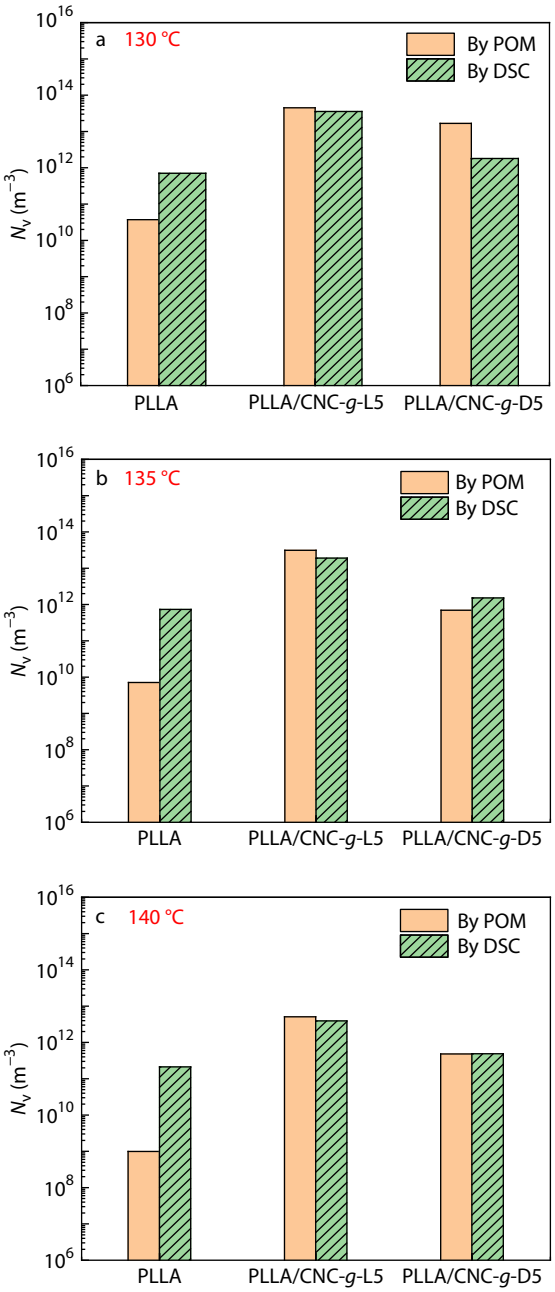

Fig. 11 The nucleation density calculated from the DSC data and directly observed from the POM images at (a) 130 °C, (b) 135 °C and (c) 140 °C.

features in WAXD and FTIR spectra. The interfacial sc-PLA contributes to the improvement of rheological properties with enhanced melt strength and prominent shear thinning effect. In melt crystallization process, CNC-*g*-L possesses more effective nucleation and less restriction to chain mobility than CNC-*g*-D at the undercooled condition, leading to the markedly improved crystallization kinetics in the PLLA/CNC-*g*-L nanocomposites. Our work could be instructive and contributable to the development of high-performance nanocomposites of polylactide and cellulose nanocrystals.

NOTES

The authors declare no competing financial interest.

Electronic Supplementary Information

The electronic supplementary information is available free of charge in the online version of this article at https://doi.org/10.1007/s10118-021-2635-7.

ACKNOWLEDGMENTS

This work was financially supported by the National Natural Science Foundation of China (Nos. 51503055 and 51673056) and the Fundamental Research Funds for the Central Universities (No. PA2020GDKC0009).

REFERENCES

1 Drumright, R. E.; Gruber, P. R.; Henton, D. E. Polylactic acid technology. *Adv. Mater.* **2000**, *12*, 1841–1846.
2 Wang, L.; Lee, R. E.; Wang, G.; Chu, R. K. M.; Zhao, J.; Park, C. B. Use of stereocomplex crystallites for fully-biobased microcellular low-density poly(lactic acid) foams for green packaging. *Chem. Eng. J.* **2017**, *327*, 1151–1162.
3 Nofar, M.; Ameli, A.; Park, C. B. Development of polylactide bead foams with double crystal melting peaks. *Polymer* **2015**, *69*, 83–94.
4 Nagarajan, V.; Mohanty, A. K.; Misra, M. Perspective on polylactic acid (PLA) based sustainable materials for durable applications: Focus on toughness and heat resistance. *ACS Sustain. Chem. Eng.* **2016**, *4*, 2899–2916.
5 Wang, Q. J.; Zhang, J.; Wang, X. H.; Wang, Z. G. Significant enhancement of notched Izod impact strength of PLA-based blends through encapsulating PA11 particles of low amounts by EGMA elastomer. *Appl. Surf. Sci.* **2020**, *526*, 146657.
6 Bai, J.; Fang, H.; Zhang, Y.; Wang, Z. Studies on crystallization kinetics of bimodal long chain branched polylactides. *CrystEngComm* **2014**, *16*, 2452–2461.
7 Li, C.; Luo, S.; Wang, J.; Wu, H.; Guo, S.; Zhang, X. Conformational regulation and crystalline manipulation of PLLA through a self-assembly nucleator. *Biomacromolecules* **2017**, *18*, 1440–1448.
8 Cheng, L.; Hu, C.; Li, J.; Huang, S.; Jiang, S. Stereocomplex-affected crystallization behaviour of PDLA in PDLA/PLDLA blends. *CrystEngComm* **2019**, *21*, 329–338.
9 Wang, B.; Wen, T.; Zhang, X.; Tercjak, A.; Dong, X.; Müller, A. J.; Wang, D.; Cavallo, D. Nucleation of poly(lactide) on the surface of different fibers. *Macromolecules* **2019**, *52*, 6274–6284.
10 Gong, X.; Pan, L.; Tang, C. Y.; Chen, L.; Li, C.; Wu, C.; Law, W. C.; Wang, X.; Tsui, C. P.; Xie, X. Investigating the crystallization behavior of poly(lactic acid) using CdSe/ZnS quantum dots as heterogeneous nucleating agents. *Compos. Part B: Eng.* **2016**, *91*, 103–110.
11 Sun, X.; Xue, B.; Yang, S. D.; Huo, K. W.; Liao, X. Y.; Li, X. J.; Xie, L.; Qin, S. H.; Zheng, Q. Structural conversion of PLLA/ZnO composites facilitated by interfacial crystallization to potential application in oil-water separation. *Appl. Surf. Sci.* **2020**, *517*, 146135.
12 Kulinski, Z.; Piorkowska, E. Crystallization, structure and properties of plasticized poly(L-lactide). *Polymer* **2005**, *46*,

10290–10300.
13 Okamoto, K.; Ichikawa, T.; Yokohara, T.; Yamaguchi, M. Miscibility, mechanical and thermal properties of poly(lactic acid)/polyester-diol blends. *Eur. Polym. J.* **2009**, *45*, 2304–2312.
14 Dufresne, A. Cellulose nanomaterial reinforced polymer nanocomposites. *Curr. Opin. Colloid. In.* **2017**, *29*, 1–8.
15 Huang, S.; Zhou, L.; Li, M. C.; Wu, Q.; Zhou, D. Cellulose nanocrystals (CNCs) from corn stalk: activation energy analysis, Materials 2017, 80.
16 Qiu, Y.; Lv, Q.; Wu, D.; Xie, W.; Peng, S.; Lan, R.; Xie, H. Cyclic tensile properties of the polylactide nanocomposite foams containing cellulose nanocrystals. *Cellulose* **2018**, *25*, 1795–1807.
17 Tan, K.; Heo, S.; Foo, M.; Chew, I. M.; Yoo, C. An insight into nanocellulose as soft condensed matter: challenge and future prospective toward environmental sustainability. *Sci. Total. Environ.* **2019**, *650*, 1309–1326.
18 Matouk, Z.; Torriss, B.; Rincon, R.; Dorris, A.; Beck, S.; Berry, R. M.; Chaker, M. Functionalization of cellulose nanocrystal films using non-thermal atmospheric-Pressure plasmas. *Appl. Surf. Sci.* **2020**, *511*, 145566.
19 Zhou, L.; He, H.; Li, M.; Huang, S.; Mei, C.; Wu, Q. Enhancing mechanical properties of poly(lactic acid) through its *in-situ* crosslinking with maleic anhydride-modified cellulose nanocrystals from cottonseed hulls. *Ind. Crop. Prod.* **2018**, *112*, 449–459.
20 Yin, Y.; Lucia, L. A.; Pal, L.; Jiang, X.; Hubbe, M. A. Lipase-catalyzed laurate esterification of cellulose nanocrystals and their use as reinforcement in PLA composites. *Cellulose* **2020**, *27*, 6263–6273.
21 Shojaeiarani, J.; Bajwa, D. S.; Hartman, K. Esterified cellulose nanocrystals as reinforcement in poly(lactic acid) nanocomposites. *Cellulose* **2019**, *26*, 2349–2362.
22 Vatansever, E.; Arslan, D.; Nofar, M. Polylactide cellulose-based nanocomposites. *Int. J. Biol. Macromol.* **2019**, *137*, 912–938.
23 Bondeson, D.; Oksman, K. Dispersion and characteristics of surfactant modified cellulose whiskers nanocomposites. *Compos. Interfaces* **2012**, *14*, 617–630.
24 Kim, J.; Montero, G.; Habibi, Y.; Hinestroza, J. P.; Genzer, J.; Argyropoulos, D. S.; Rojas, O. J. Dispersion of cellulose crystallites by nonionic surfactants in a hydrophobic polymer matrix. *Polym. Eng. Sci.* **2009**, *49*, 2054–2061.
25 Larsson, E.; Sanchez, C. C.; Porsch, C.; Karabulut, E.; Wågberg, L.; Carlmark, A. Thermo-responsive nanofibrillated cellulose by polyelectrolyte adsorption. *Eur. Polym. J.* **2013**, *49*, 2689–2696.
26 Martins, N. C. T.; Freire, C. S. R.; Pinto, R. J. B.; Fernandes, S. C. M.; Pascoal, Neto C.; Silvestre, A. J. D.; Causio, J.; Baldi, G.; Sadocco, P.; Trindade, T. Electrostatic assembly of Ag nanoparticles onto nanofibrillated cellulose for antibacterial paper products. *Cellulose* **2012**, *19*, 1425–1436.
27 Moon, R. J.; Martini, A.; Nairn, J.; Simonsen, J.; Youngblood, J. Cellulose nanomaterials review: structure, properties and nanocomposites. *Chem. Soc. Rev.* **2011**, *40*, 3941–3994.
28 Habibi, Y. Key advances in the chemical modification of nanocelluloses. *Chem. Soc. Rev.* **2014**, *43*, 1519–1542.
29 Fotie, G.; Gazzotti, S.; Ortenzi, M. A.; Piergiovanni, L. Implementation of high gas barrier laminated films based on cellulose nanocrystals for food flexible packaging. *Appl. Sci.* **2020**, *10*, 3201.
30 Andresen, M.; Johansson, L. S.; Tanem, B. S.; Stenius, P. Properties and characterization of hydrophobized microfibrillated cellulose. *Cellulose* **2006**, *13*, 665–677.
31 Kloser, E.; Gray, D. G. Surface grafting of cellulose nanocrystals with poly(ethylene oxide) in aqueous media. *Langmuir* **2010**, *26*, 13450–13456.
32 Goffin, A. L.; Raquez, J. M.; Duquesne, E.; Siqueira, G.; Habibi, Y.; Dufresne, A.; Dubois, P. From interfacial ring-opening polymerization to melt processing of cellulose nanowhisker-filled polylactide-based nanocomposites. *Biomacromolecules* **2011**, *12*, 2456–2465.
33 Lizundia, E.; Fortunati, E.; Dominici, F.; Vilas, J. L.; Leon, L. M.; Armentano, I.; Torre, L.; Kenny, J. M. PLLA-grafted cellulose nanocrystals: Role of the CNC content and grafting on the PLA bionanocomposite film properties. *Carbohydr. Polym.* **2016**, *142*, 105–113.
34 de Paula, E. L.; Roig, F.; Mas, A.; Habas, J. P.; Mano, V.; Pereira, F. V.; Robin, J. J. Effect of surface-grafted cellulose nanocrystals on the thermal and mechanical properties of PLLA based nanocomposites. *Eur. Polym. J.* **2016**, *84*, 173–187.
35 Habibi, Y.; Aouadi, S.; Raquez, J. M.; Dubois, P. Effects of interfacial stereocomplexation in cellulose nanocrystal-filled polylactide nanocomposites. *Cellulose* **2013**, *20*, 2877–2885.
36 Gupta, A.; Katiyar, V. Cellulose functionalized high molecular weight stereocomplex polylactic acid biocomposite films with improved gas barrier, thermomechanical properties. *ACS Sustain. Chem. Eng.* **2017**, *5*, 6835–6844.
37 Wu, H.; Nagarajan, S.; Zhou, L.; Duan, Y.; Zhang, J. Synthesis and characterization of cellulose nanocrystal-graft-poly(D-lactide) and its nanocomposite with poly(L-lactide). *Polymer* **2016**, *103*, 365–375.
38 Wang, H.; Yu, J.; Fang, H.; Wei, H.; Wang, X.; Ding, Y. Largely improved mechanical properties of a biodegradable polyurethane elastomer *via* polylactide stereocomplexation. *Polymer* **2018**, *137*, 1–12.
39 Xie, Q.; Wang, S.; Chen, X.; Zhou, Y.; Fang, H.; Li, X.; Cheng, S.; Ding, Y. Thermal stability and crystallization behavior of cellulose nanocrystals and their poly(L-lactide) nanocomposites: effects of surface ionic group and poly(D-lactide) grafting. *Cellulose* **2018**, *25*, 6847–6862.
40 Fang, H.; Chen, X.; Wang, S.; Cheng, S.; Ding, Y. Enhanced mechanical and oxygen barrier performance in biodegradable polyurethanes by incorporating cellulose nanocrystals with interfacial polylactide stereocomplexation. *Cellulose* **2019**, *26*, 9751–9764.
41 Garlotta, D. A literature review of poly(lactic acid). *J. Polym. Environ.* **2001**, *9*, 63–84.
42 Chen, X.; Han, L.; Zhang, T.; Zhang, J. Influence of crystal polymorphism on crystallinity calculation of poly(L-lactic acid) by infrared spectroscopy. *Vib. Spectrosc.* **2014**, *70*, 1–5.
43 Ma, P.; Jiang, L.; Xu, P.; Dong, W.; Chen, M.; Lemstra, P. J. Rapid stereocomplexation between enantiomeric comb-shaped cellulose-*g*-poly(L-lactide) nanohybrids and poly(D-lactide) from the melt. *Biomacromolecules* **2015**, *16*, 3723–3729.
44 Saeidlou, S.; Huneault, M. A.; Li, H.; Park, C. B. Poly(lactic acid) crystallization. *Prog. Polym. Sci.* **2012**, *37*, 1657–1677.
45 Ying, Z.; Wu, D.; Wang, Z.; Xie, W.; Qiu, Y.; Wei, X. Rheological and mechanical properties of polylactide nanocomposites reinforced with the cellulose nanofibers with various surface treatments. *Cellulose* **2018**, *25*, 3955–3971.
46 Arias, A.; Heuzey, M.-C.; Huneault, M. A.; Ausias, G.; Bendahou, A. Enhanced dispersion of cellulose nanocrystals in melt-processed polylactide-based nanocomposites. *Cellulose* **2015**, *22*, 483–498.
47 Besbes, I.; Alila, S.; Boufi, S. Nanofibrillated cellulose from TEMPO-oxidized eucalyptus fibres: effect of the carboxyl content. *Carbohydr. Polym.* **2011**, *84*, 975–983.
48 Muiruri, J. K.; Liu, S.; Teo, W. S.; Kong, J.; He, C. Highly

biodegradable and tough polylactic acid-cellulose nanocrystal composite. *ACS Sustain. Chem. Eng.* **2017**, *5*, 3929–3937.
49 Liu, H.; Bai, D.; Bai, H.; Zhang, Q.; Fu, Q. Constructing stereocomplex structures at the interface for remarkably accelerating matrix crystallization and enhancing the mechanical properties of poly(L-lactide)/multi-walled carbon nanotube nanocomposites. *J. Mater. Chem. A* **2015**, *3*, 13835–13847.
50 Mano, J. o. F.; Wang, Y.; Viana, J. l. C.; Denchev, Z.; Oliveira, M. J. Cold crystallization of PLLA studied by simultaneous SAXS and WAXS. *Macromol. Mater. Eng.* **2004**, *289*, 910–915.
51 Xu, C.; Lv, Q.; Wu, D.; Wang, Z. Polylactide/cellulose nanocrystal composites: a comparative study on cold and melt crystallization. *Cellulose* **2017**, *24*, 2163–2175.
52 Liang, Y.; Xu, J.; Li, Y.; Zhong, G.; Wang, R.; Li, Z. Promoting interfacial transcrystallization in polylactide/ramie fiber composites by utilizing stereocomplex crystals. *ACS Sustain. Chem. Eng.* **2017**, *5*, 7128–7136.
53 Zhang, Y.; Xu, Z.; Wang, Z.; Ding, Y.; Wang, Z. Strong enhancements of nucleation and spherulitic growth rates through amplified interfacial effects for immiscible linear polymer/comb-like copolymer double-layer films. *RSC Adv.* **2014**, *4*, 20582–20591.
54 Zhang, Y..; Wang, Z. Increased spherulitic growth rates of semicrystalline polymer due to enhanced limited local chain segmental mobility at the interface of double-layer thin films. *Chinese J. Polym. Sci.* **2013**, *31*, 1276–1283.
55 Housmans, J. W.; Steenbakkers, R. J. A.; Roozemond, P. C.; Peters, G. W. M.; Meijer, H. E. H. Saturation of pointlike nuclei and the transition to oriented structures in flow-induced crystallization of isotactic polypropylene. *Macromolecules* **2009**, *42*, 5728–5740.
56 Fang, H.; Zhang, Y.; Bai, J.; Wang, Z. Shear-induced nucleation and morphological evolution for bimodal long chain branched polylactide. *Macromolecules* **2013**, *46*, 6555–6565.

https://doi.org/10.1007/s10118-021-2635-7